Energy Conversion and Management 353 (2026) 121154

Contents lists available at ScienceDirect

Energy Conversion and Management

journal homepage: www.elsevier.com/locate/enconman

Energy, exergy and mass balances of a biomass pyrolysis pilot plant

César Gracia-Monforte [a,*], Alejandro Lete [a], Frédéric Marias [b], Javier Ábrego [a], Jesús Arauzo [a]

[a] Thermochemical Processes Group (GPT), Aragon Institute for Engineering Research (I3A), University of Zaragoza 50018 Zaragoza, Spain
[b] Universite de Pau et des Pays de l'Adour, E2S UPPA, LaTEP, Pau, France

ARTICLE INFO

Keywords:
Pyrolysis
Biomass
Energy balance
Exergy balance
Heat recovery
Pilot plant

ABSTRACT

This work presents the methodology and results of the energy, exergy, and mass balances of a fixed-bed downdraft biomass pyrolysis pilot plant. The analysis covers different operating modes: pyrolysis without energy recovery, with energy recovery from products, and with combustion of non-condensable gases including exhaust-gas heat recovery. The proposed framework enables consistent comparison of energy and exergy performance under varying process configurations. Experimental results show that the external heat demand of the pyrolysis process strongly depends on the energy recovery strategy. When products are cooled to the reference state, the required heat input is approximately 1.3 MJ/kg, increasing to about 3 MJ/kg when products leave at the pyrolysis temperature. The combustion of process gases significantly reduces this demand, while integrating exhaust-gas heat recovery leads to quasi-autothermal operation. Exergy analysis reveals that gas combustion and heat recovery lower exergy efficiency due to the conversion of high-quality pyrogases into exhaust gases. Nevertheless, the methodology developed allows quantifying these trade-offs and provides a comprehensive tool to evaluate process integration strategies in biomass pyrolysis systems aimed at improved thermal performance and sustainability.

1. Introduction

Pyrolysis is an emergent and versatile thermochemical option for valorizing renewable biomass resources. Under limited oxygen supply and moderate temperatures, lignocellulosic biomass pyrolysis yields three main product streams: solid biochar, condensable vapors (bio-oil), and permanent gases. The first two product fractions are of great interest due to their distinct roles in environmental management, energy systems and even chemical industry. Biochar can simultaneously enable long-term carbon sequestration and soil amendment, and its application is regarded as a negative-emission strategy pathway. Bio-oil is a liquid renewable fuel and chemical precursor, with high energy density compared to raw biomass and the potential for partial substitution of fossil-derived products. Finally, non-condensable pyrolytic gases are usually combusted within the process to provide −total or partially- the necessary heat for pyrolysis. Several reviews have highlighted the relevance of reactor design and operating conditions in shaping these three fractions [1–4].

For any of the proposed applications of pyrolysis products, the energy balance of the system is pivotal both in terms of energy efficiency and carbon capture. If bio-oil is intended to partially displace fossil fuels, the net energy efficiency of the process is of utmost importance. If significant fractions of the feedstock must be consumed merely to maintain reactor temperatures, the effective energy yield of bio-oil decreases. From the perspective of carbon capture, if additional biomass must be combusted externally to sustain pyrolysis, the net carbon sequestration benefit is reduced. The energy balance becomes even more critical if, instead of additional biomass, other non-renewable energy sources are applied to maintain quasi-autothermal operation of the pyrolysis system. In this regard, integrating pyrolysis into combined heat and power systems has been proposed as a strategy to improve overall efficiency [5–7].

For various reaction systems, a number of studies in literature have quantified the heat demand of pyrolysis. From thermogravimetric analysis (TGA) or small lab-scale experiments, it is well established that biomass decomposition is globally endothermic, although transient exothermic events can occur depending on feedstock composition and heating rate. Crombie and Mašek found that in a fixed bed batch pyrolysis unit above ~450 °C the energy content of the non-condensable gases alone was sufficient to sustain pyrolysis without recourse to external fuel [8]. Ábrego et al. reported similar figures for beech wood

* Corresponding author.
E-mail address: c.gracia@unizar.es (C. Gracia-Monforte).

https://doi.org/10.1016/j.enconman.2026.121154
Received 21 October 2025; Received in revised form 8 January 2026; Accepted 30 January 2026
Available online 4 February 2026

Nomenclature

AP	organic aqueous phase of the bio-oil
Cp	specific heat capacity at constant pressure, $MJ \bullet kg^{-1} \bullet K^{-1}$
e	specific exergy, $MJ \bullet kg^{-1}$
GC–MS	gas chromatography–mass spectrometry
h	specific enthalpy, $MJ \bullet kg^{-1}$
HHV	higher heating value, $MJ \bullet kg^{-1}$
HP	organic heavy phase of the bio-oil
hy	hydrogen in wt.%, dry basis
LHV	lower heating value, $MJ \bullet kg^{-1}$
m	mass, kg
moist	moisture in wt.%, wet basis
OAP	organic compounds of the aqueous phase
OC	oxygen carrier
OHP	organic compounds of the aqueous phase
P	pressure, Pa
Q	enthalpy required, $MJ \bullet kg^{-1}$
R	universal gas constant, 8.314472 $kJ \bullet mol^{-1} \bullet K^{-1}$
s	specific entropy, $MJ \bullet kg^{-1}$
STP	standard temperature and pressure at 298.15 K and $1.01 \bullet 10^5$ Pa
T	temperature, K
TGA	thermogravimetric analysis
y	mass fraction, wt.%

Greek letters

Δ	difference
η	overall energetic yield, %
ψ	exergetic efficiency, %
λ	latent heat of vaporizarion, $MJ \bullet kg^{-1}$
φ	ratio of standard specific chemical exergy
ρ	density, kg/m^3

Subscripts

0	at 298.15 K and $1.01 \bullet 10^5$ Pa
biochar	biochar
biomass	biomass
bio-oil	bio-oil
ch	chemical
comb	combustion
db	dry basis
element	element (C, H, O, N, S)
f	formation
gas	pyrolysis gas
$H_2O_{(v)}$	steam
i	biochar, bio-oil and pyrogases
input	inlet streams to the control volume
j	water in the bio-oil, AP and HP
k	OAP and OHP
l	H_2, N_2, CH_4, CO, CO_2, C_2H_2, C_2H_4 and C_2H_6.
loss	loss
m	CO_2 and steam
moist	moisture
n	CO_2, CO, NO and SO_2.
output	outflow streams from the control volume
ph	physical
process	process
pyr	pyrolysis
pyrogases	non-condensable gases of the pyrolysis process
Q	heat required
solid	solid (biomass and biochar)
water	water

Superscripts

0	at 298.15 K and $1.01 \bullet 10^5$ Pa

pyrolysis in a fixed-bed reactor [9]. Jerzak et al. reviewed the heat requirements of fixed-bed, screw-conveyor, and fast pyrolysis reactors, reporting values in the range of 0.5–3.0 MJ kg^{-1} depending on operating mode (continuous or discontinuous), reactor (fixed bed, Auger of fluidized bed), heating rate (slow or fast pyrolysis) or the use of a gas carrier, and also provided experimental data for intermediate pyrolysis [10–12] which were in the range 0.8–2.0 MJ/kg depending additionally on the biomass feedstock [13]. From all these results, it is clear that efficient heat integration can play a significant role in the performance of pyrolysis systems [14].

Nevertheless, a thorough analysis of pyrolysis systems should not only take into account the energy balance alone. Exergy analysis is capable of revealing low quality, degraded' energy flows with limited usability. For instance, for bio-oil production, an energy balance alone may suggest that the process is efficient, yet much of the energy might be recovered in low-temperature heat streams or in combustion gases, with limited potential to substitute for high-grade fossil fuels. Also, as an example, in the case of biochar any additional combustion of biomass to supply heat reduces the fraction of carbon sequestered. Exergy analysis would help quantify the penalty of such internal fuel use by distinguishing between the destruction of high-quality chemical exergy in biochar and the generation of low-grade thermal exergy for process heating. In fact, biochar retains a significant fraction of the feedstock's chemical exergy in the form of recalcitrant, aromatic carbon structures. This is energy that is not degraded into low-quality heat or CO_2 during pyrolysis [15]. All these potential exergy losses can reveal optimal routes for heat integration. Pioneering work has shown how to calculate chemical exergy of pyrolysis products directly from elemental composition [16], and more recent studies have applied exergoeconomic approaches to different biomass feedstocks [17,18].

Only a limited number of studies explicitly account for exergy destruction within reactors, condensers, and auxiliary units, despite its relevance for comparing biomass pyrolysis with alternative bioenergy pathways such as gasification or anaerobic digestion [15]. Recent exergy-based analyses of biomass pyrolysis systems have provided new insights into the distribution and quality of energy and exergy among product streams, as well as the influence of operating conditions on gas, bio-oil, and biochar performance [19–21]. Related studies on biomass thermochemical conversion processes, such as torrefaction, have highlighted similar considerations regarding exergy efficiency and energy quality degradation [15]. Comparative assessments across thermochemical technologies, including pyrolysis, gasification, and combustion, report substantial differences in exergy efficiency and irreversibilities [22–24], while broader reviews emphasize the need for consistent methodologies and benchmarking frameworks in biomass exergy analysis [25]. More recent contributions have also explored emerging concepts, such as microwave-assisted pyrolysis, further advancing the understanding of exergy distribution and efficiency [26]. Nevertheless, most existing exergy analyses of biomass pyrolysis rely on theoretical models or single process configurations, limiting direct experimental comparison between alternative integration strategies. While some qualitative trends derived from exergy analysis are well established from thermodynamic theory, the contribution of this work lies in the experimental quantification and consistent comparison of energy and exergy performance across different integration strategies applied to a pilot-scale downdraft biomass pyrolysis reactor.

While some qualitative trends derived from exergy analysis are well established from thermodynamic theory, the contribution of this work

lies in the experimental quantification and consistent comparison of energy and exergy performance across different integration strategies applied to a pilot-scale downdraft biomass pyrolysis reactor.

Thus, this paper aims to analyze the effect, both in terms of energy and exergy, of different scenarios: first, pyrolysis with energy recovery from the products, and second, combusting the pyrolysis gases to provide the required process heat, with the hot exhaust gases subsequently utilized to preheat both the combustion air and the biomass feed. Both scenarios are compared against a base case where no heat is recovered from the products.

2. Experimental section and methodology

This section includes the results obtained in the different experiments carried out, the three different scenarios for the energy and exergy balances and the methodology used for the calculations.

2.1. Feedstock and pyrolysis by-products characterization

2.1.1. Biomass characterization

The biomass used for the experiments is beech wood chips. The proximate analysis determined moisture, ash and volatile matter contents in accordance with UNE-EN-14774-3:2010, UNE-EN ISO 18122:2016, and UNE-EN ISO 18123:2016 standards, respectively, while fixed carbon was obtained by difference. The ultimate analysis quantified the elemental composition (C, H, N, S) using a Leco CHN 628 analyzer equipped with the Sulphur Addon module, and oxygen content was calculated by difference. The higher heating value (HHV) was determined with an IKA C2000 basic bomb calorimeter. Calorific value, proximate and ultimate analysis results of the biomass are provided in Table 1. These values fall within the typical ranges reported for biomass [27,28], with a comparatively low fixed carbon content, slightly higher-than-average volatiles, and a low ash fraction. The quantified sulfur is negligible, while the sample also exhibits a very low nitrogen content and a relatively high oxygen content. Biomass feedstock characterization data reported in Table 1 constitute the basis for the energy and exergy balance calculations presented in this study.

2.1.2. Characterization of pyrolysis by-products

The two biochars obtained from the pyrolysis process were characterized. Each biochar was subjected to proximate analysis to assess the moisture, volatile matter, and ash content following the standards ISO 18134-1:2015, ISO 18123:2015, and ISO 18122:2015, respectively. The lower heating value (LHV) was determined with an IKA-WERKE C2000 Basic Calorimeter. In addition, elemental analysis (C, H, and N contents) was performed with a Leco CHN 628 analyzer. Textural properties of the biochars, including specific surface area, pore volume, and pore size, were assessed by N_2 adsorption–desorption isotherms at 77 K in a Micromeritics equipment using the BET equation.

The pyrolysis liquids (bio-oil) were analyzed to determine their composition. Firstly, the bio-oil was decanted to separate the aqueous fraction from the organic fraction. The water content was quantified by Karl Fischer titration in a Mettler Toledo V20 KF Titrator. The chemical composition of the bio-oil was determined by gas chromatography–mass spectrometry (GC–MS) Agilent Serie 7890A, enabling identification of the main families of organic compounds present. The organic fraction of the bio-oil was characterized to determine its elemental composition and energy content. CHN elemental analysis was performed to quantify the C, H, and N contents, while the LHV was measured. The same equipment used for the characterization of the biochar was employed in both analyses.

Table 1
Proximate, ultimate analysis and heating value of the biomass.

Proximate analysis (wt.%, wet basis)	
Moisture	9.2 ± 0.4
Ash	1.0 ± 0.1
Volatiles	79.7 ± 0.2
Fixed carbon[(a)]	10.1 ± 0.4
Ultimate analysis (wt.%, wet basis)	
C	46.3 ± 0.1
H	6.5 ± 0.1
N	0.1 ± 0.1
S	0.0 ± 0.0
O[(b)]	46.1 ± 0.1
Heating values (wet basis)	
HHV_{MW} (MJ/kg)	17.8 ± 0.1
LHV_{MW} [(c)] (MJ/kg)	16.3 ± 0.1

[(a)] Calculated by difference (wt.%): Fixed carbon = 100 – Moisture – Ash – Volatiles
[(b)] Calculated by difference (wt.%): O = 100 – C – H – N – S – Ash
[(c)] LHV calculated as: $LHV = HHV - 24.49 \bullet (moist + 9 \bullet hy \bullet (1 - moist/100))$; where *HHV* is the value obtained experimentally, *moist* is the moisture and *hy* is the hydrogen obtained in the ultimate analysis in dry basis.

2.2. Experimental system

The pilot plant where the experiments were carried out is located at the Aragon Institute for Engineering Research (I3A), within the Thermochemical Processes Group (GPT) at University of Zaragoza (Fig. 1) (Fig. 2). The facility is capable of processing up to 15 kg/h of biomass, although the feeding rate in this work was 3 kg/h. The biomass used in the process consisted of beech wood chips of size class P16, classified according to the UNE-EN ISO 17225-4:2021 standard. In some references, this same size is also referred to as the designation G30, according to the Austrian Önorm M7133 standard, which was widely used in Central Europe and has been replaced by the ISO 17225 specification.

The chips are loaded into the hopper, located at the top of the plant. From there, they are fed into the reactor by means of a screw feeder. The

Fig. 1. Pyrolysis pilot plant in the GPT facilities.

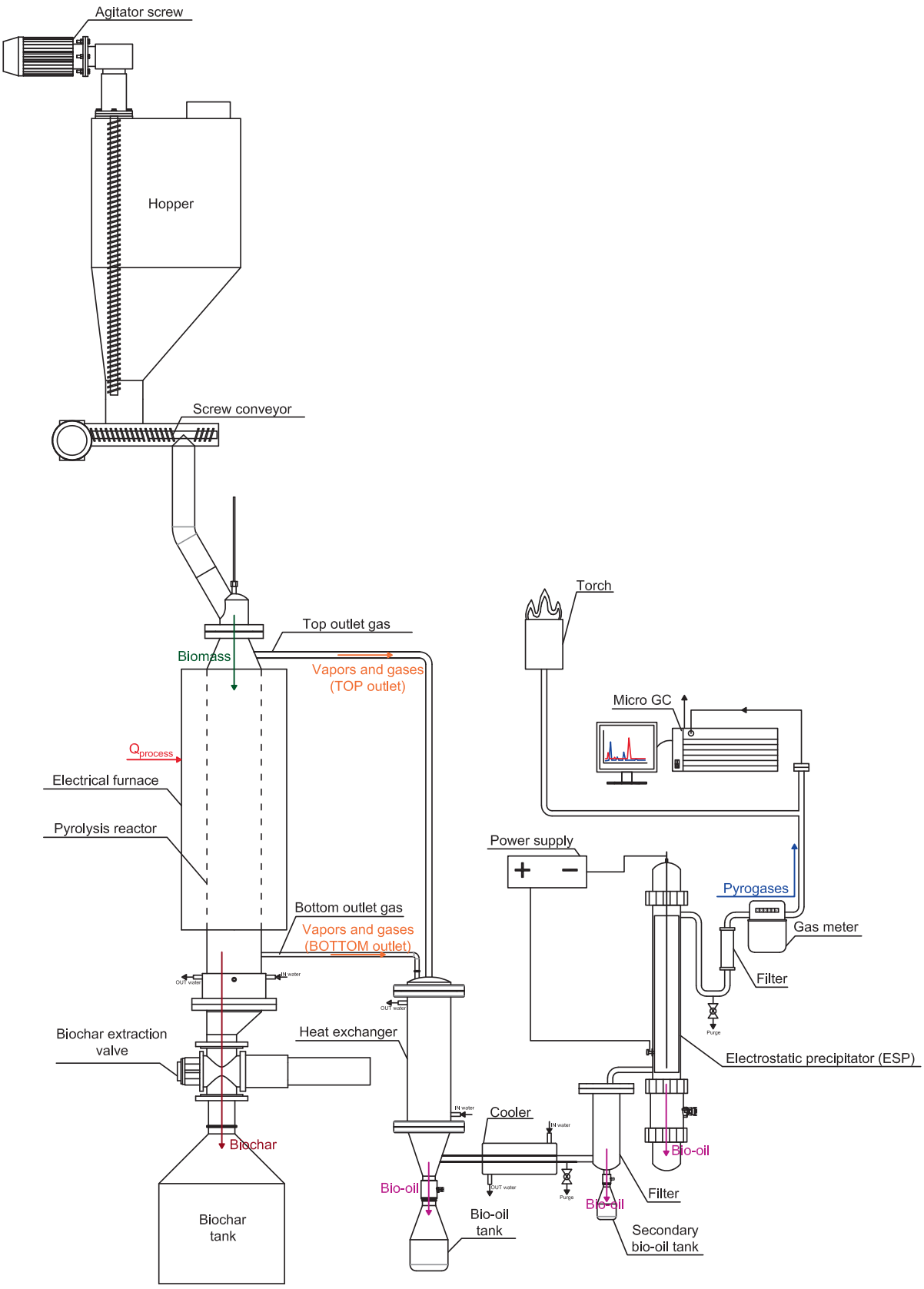

Fig. 2. P&ID of the pyrolysis plant.

biomass enters the reactor from the top and falls freely until it reaches the bed. A small nitrogen flowrate is also introduced in order to prevent any gases to flow upwards to the feeding system. In addition, the hopper is equipped with an agitator that facilitates the downward flow of the chips towards the screw feeder. Both the screw feeder and the agitator can be operated at variable speeds, which makes it possible to regulate the biomass mass flow rate into the reactor.

Inside the pyrolysis reactor, a bed of previously pyrolyzed biomass (char) is maintained. As new biomass is introduced, pyrolysis takes place in the upper part of the bed, where the reaction front is located. The reactor is externally heated by an electric furnace, and along its central axis a multi-thermocouple probe is installed to measure temperatures at different heights. The biomass entering the reactor undergoes thermal degradation into char, pyrolysis liquid (bio-oil), and pyrolysis gases, with the liquids leaving the reactor in vapor form due to the high operating temperatures. The reactor has two options for the outlet of gases and vapors: one at the top and another at the bottom. Char is extracted through a rotary valve located at the reactor outlet. Just above the valve, a small cooling jacket (char cooler) allows the lower part of the reactor to be water-cooled when the temperature becomes too high in that section. The operation of this cooling jacket is governed by one of the thermocouples, the aim is to maintain this section within the range of 150–200 °C to avoid undesired condensation. There is still a safety margin, since the rotary valve can withstand temperatures up to 400 °C.

Small amounts of nitrogen are also injected at the bottom of the reactor, with the same purpose as in the hopper: to prevent condensation of vapors and assist their transport toward the gas outlet. In this area, a differential pressure sensor is installed, measuring the difference between the internal pressure of the reactor and the atmospheric pressure. The differential pressure is typically small, in the range of 1.02 to 1.2 bar, depending on whether pyrolysis gases are being generated.

The gases are then directed to a shell-and-tube heat exchanger cooled by a chiller with a water–ethylene glycol mixture. At this stage, most of the vapors condense and the majority of the bio-oil is collected. Downstream of this exchanger, the gas passes through a secondary cooling jacket, a filtering bed, and an electrostatic precipitator (ESP) for final cleaning, where the remaining bio-oil that did not condense in the first exchanger is recovered. The cleaned gas is analyzed using a micro gas chromatograph Agilent 990, which allows determination of its volumetric composition. In addition, a flow meter is used to measure the gas flow rate. Finally, the gases are directed to a flare. However, in this study, the focus is on evaluating the energy that could be obtained from their combustion to supply the heat required for the pyrolysis process.

2.2.1. Experiments carried out

Two configurations where the gas outlet of the pyrolysis reactor change have been studied. In the first block of the experiments, three experiments were carried out extracting gases and vapors by the outlet located at the lower part of the reactor. The second block collects the three experiments where the outlet gas and vapors were extracted from the upper part of the reactor. Finally, a long experiment of 10 h was performed with the top outlet configuration, since this configuration, as will be mentioned afterwords, was the one that offered best results. Table 2, summarizes the operational conditions of the experiments performed.

Table 2
Experimental conditions for top and bottom outlet configurations.

Outlet gas configuration	Repetitions	T [°C]	Feed mass flow [kg/h]	Duration [h]
Bottom	3	600	3	3
Top	3	600	3	3
Top	1	600	3	10

2.3. Scenarios

Three different scenarios have been analyzed for the calculation of the energy and exergy balances of the process.

2.3.1. Pyrolysis

Two scenarios were studied for pyrolysis. The results for the mass balance of all experiments are summarized in Table 3. Beech wood chips were selected as feedstock due to their relatively homogeneous composition, wide availability in European forestry residues, and frequent use as a reference hardwood in experimental biomass pyrolysis studies [1,9,29,30]. Several recent experimental investigations have reported the pyrolysis behavior, product yields, and thermal decomposition characteristics of beech wood and similar hardwoods under conditions relevant to slow and intermediate pyrolysis. The selected operating temperature falls within the range commonly adopted for conventional biomass pyrolysis, where extensive devolatilization is achieved while preserving biochar structure and quality, as documented in recent comprehensive reviews and experimental studies [31,32]. Therefore, both the chosen feedstock and operating temperature are considered representative of biomass pyrolysis systems reported in the literature. In Case A (see Fig. 3) shows the pyrolysis carried out at 600 °C in the downdraft pyrolysis reactor. Pyrolysis products are assumed to leave the control volume at the standard reference state, i.e., heat is assumed to be recovered. Case A represents an idealized upper-bound scenario, assuming full recovery of the heat released during product cooling. This configuration is not intended to describe a directly implementable system, but to provide a theoretical benchmark against which more realistic configurations can be compared. On the other hand, Fig. 4 shows Case B, when the pyrolysis process products leave the control volume at the pyrolysis temperature (T_{pyr}). In both cases, three fractions are obtained from biomass pyrolysis. A solid fraction (biochar), the non-condensable gases from pyrolysis (pyrogases) and the liquid fraction. The liquid fraction (bio-oil) consists of a mixture of water and organic compounds. Due to the immiscibility between phases, the bio-oil can be separated by decantation into an aqueous phase and an organic phase. For the purpose of the energy and exergy analysis, the liquid products were further subdivided into three components: pure water, a heavy organic fraction (HP), and a light aqueous organic fraction (AP). Each of these three streams was treated separately in balance calculations, with the water content allocated entirely to the pure water stream and only the organic material assigned to the two organic streams. In this case, the heat is not recovered.

2.3.2. Pyrolysis with gas combustion and heat recovery

Additionally, a third scenario has been studied. This scenario considers a pyrolysis process where biochar and the bio-oil mix (water, AP and HP) were extracted at pyrolysis process conditions. The heat produced in the condensation of the liquid fraction has not been considered since it is not utilized. Therefore, liquids products are considered at pyrolysis temperature but in the scheme are shown at standard conditions, since is necessary to cool down vapors and pyrogases together for its separation. This heat is no longer recovered. After the condensation, pyrogases were burned in a combustion chamber, where they were oxidized with air. The heat released by this combustion is used to provide the required energy for sustaining the pyrolysis process. Furthermore, the hot exhaust gases leaving the combustion chamber are considered as a potential source of recoverable heat. In this work, both cases are evaluated: (i) without heat recovery from the exhaust gases (Fig. 5), and (ii) with the utilization of the exhausted gases for preheating the combustion air and the biomass feed, aiming to improve the overall energy efficiency of the system and reduce the demand for external heat supply (Fig. 6). It should be noted that, from a practical standpoint, the presence of tars and acid gases in the exhaust stream may impose additional constraints on the design and material selection of heat recovery equipment due to fouling and corrosion issues, which

Table 3
Experimental results of pyrolysis experiments. Product distribution and gas properties.

Experiment	Bot. 1	Bot. 2	Bot. 3	Average Bot.	Top 1	Top 2	Top 3	Average Top.	Long Top
Mass balance [wt.%]									
Char	33.6	35.5	32.1	33.7 ± 1.7	31.7	28.4	31.4	30.5 ± 1.9	31.1
Bio-oil	27.5	27.9	27.1	27.5 ± 0.4	30.0	28.8	30.9	29.9 ± 1.1	30.0
Pyrogases	38.9	36.6	40.8	38.8 ± 2.1	38.3	42.9	37.7	39.6 ± 2.8	38.9
Gas composition [vol.% dry basis]									
H_2	21.8	23.0	26.0	23.6 ± 2.2	26.0	28.0	28.1	27.4 ± 1.2	27.4
N_2	8.1	6.1	7.9	7.4 ± 1.1	7.0	6.2	5.2	6.1 ± 0.9	7.2
CH_4	14.6	14.9	15.2	14.9 ± 0.3	14.4	14.7	15.7	14.9 ± 0.7	15.5
CO	19.5	17.5	14.3	17.1 ± 2.6	16.1	16.6	16.3	16.3 ± 0.3	16.6
CO_2	33.7	36.4	34.5	34.9 ± 1.4	33.7	31.4	31.8	32.3 ± 1.3	31.2
C_2H_4	0.6	0.6	0.7	0.6 ± 0.1	1.6	1.9	1.6	1.7 ± 0.2	0.8
C_2H_6	1.7	1.6	1.4	1.6 ± 0.2	1.2	1.4	1.3	1.3 ± 0.1	1.3
C_2H_2	0.0	0.0	0.0	0.0 ± 0.0	0.0	0.0	0.0	0.0 ± 0.0	0.0
H_2S	0.0	0.0	0.0	0.0 ± 0.0	0.0	0.0	0.0	0.0 ± 0.0	0.0
Gas properties									
ρ_{gas} [kg/m^3]	1.10	1.10	1.05	1.08 ± 0.03	1.05	1.02	1.02	1.03 ± 0.02	1.02
LHV_{gas} [kJ/m^3(STP)]	11473.4	11380.2	11335.7	11396.4 ± 70.3	11691.0	12328.8	12493.1	12171.0 ± 423.7	11864.6
m^{3}gas/kg$_{biomass}$	0.37	0.34	0.40	0.37 ± 0.03	0.37	0.43	0.38	0.40 ± 0.03	0.39
LHV_{gas} [kJ/kg$_{biomass}$(STP)]	4214.3	3829.6	4493.4	4179.1 ± 333.3	4344.3	5320.7	4800.6	4821.9 ± 488.6	4651.9

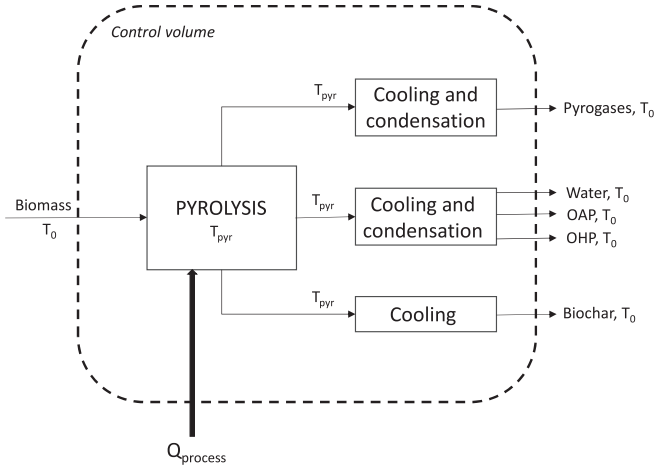

Fig. 3. Control volume for pyrolysis Case A: Products at the standard reference state.

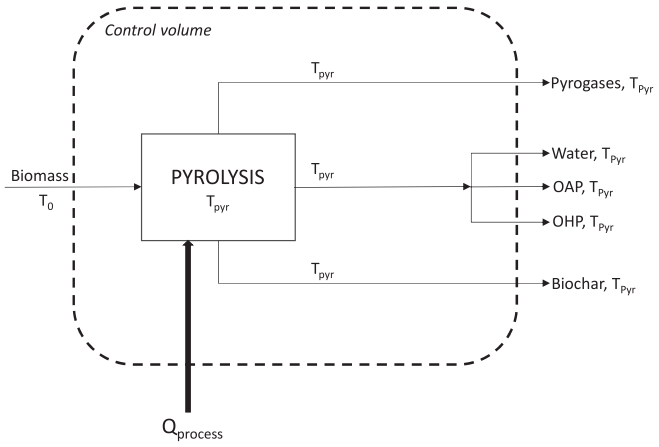

Fig. 4. Control volume for pyrolysis Case B: Products at process conditions.

would need to be addressed in industrial-scale implementations.

2.4. Assumptions

The energy and exergy balances were based on the following assumptions, simplifications, and stream properties:

- The standard reference state is $T_0 = 25$ °C and $P_0 = 1.01 \bullet 10^5$ Pa.
- Characterization of biomass is shown in Table 1, biochar is shown in Table 4 and liquids are shown in Table 5 and Table 7.
- The experimental data for the calculations have been obtained in pilot plant: mass fractions of the pyrolysis products, and pyrogases properties (volumetric composition, density and LHV) were obtained in a fixed bed pyrolysis reactor with configuration for updraft or downdraft of the outlet gases.
- Proximate and ultimate analysis of the biochar allow to calculate its specific heat capacity (Cp) value using the Hurs-Harrison method [33]. This method enables the evaluation of the contributions of each atomic element to the capacity at T_0, P_0.
- Cp for biomass and biochar was considered constant with temperature.
- All energy and exergy calculations are performed on an HHV basis; accordingly, water is considered in the liquid state at the reference conditions, while temperature-dependent sensible enthalpies of gaseous species are evaluated using NASA polynomials.
- Aqueous phase (AP) of the bio-oil is divided into the water mass fraction determined by Karl-Fischer analysis and the remaining organic fraction dissolved in it. The organic fractions dissolved in the AP is determined using GC–MS. For the organic heavy phase (OHP) the same method was followed. The major chromatographic areas of the different organic compounds were chosen for the composition of each organic phase.
- The total water fraction is considered the sum of the water of the AP and the HP.
- Liquid phases (water, AP and HP) are considered ideal solutions.
- The specific heat capacity of water and organic compounds is considered in their natural state under reference conditions for Case A, with data extracted from the CRC Handbook of Chemistry and Physics, 90th edition [34]. For Case B, everything is referenced in gas-phase based on the values of the NASA tables [35].
- Energy losses were considered as 5%, an intermediate value of other studies [36,37].
- Exergy losses were not taken into account.
- The value obtained of $Q_{process}$ in Case A, represent the most optimistic result, since is considered that the energy of the products is recovered.

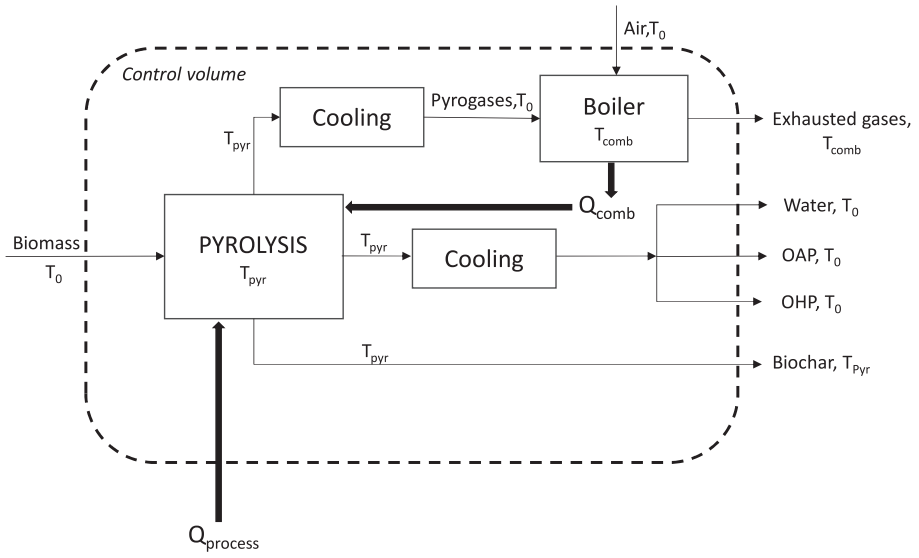

Fig. 5. Control volume for pyrolysis and combustion of pyrolysis gases. Case C (i): Pyrolysis with gas combustion without heat recovery.

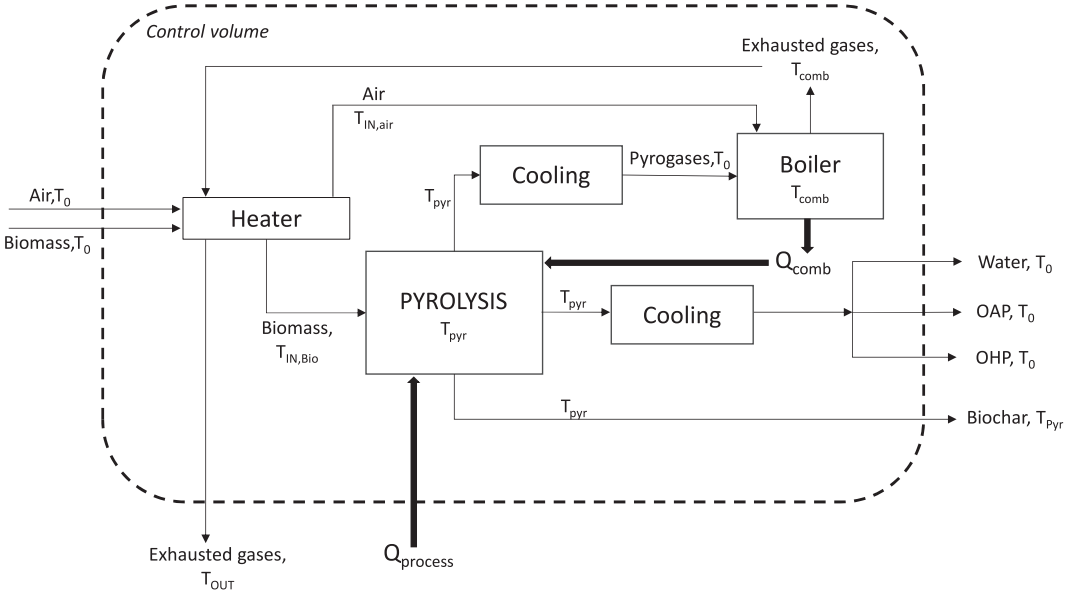

Fig. 6. Control volume for pyrolysis and combustion of pyrolysis gases. Case C (ii): Pyrolysis with gas combustion with heat recovery.

Table 4
Comparison of the proximate, ultimate analysis and textural properties of the biochar obtained at the upper and lower gas outlet.

	Moisture	Volatiles	Ash	LHV [kJ/kg]	C	H	N	O	S_{BET} [m^2/g]	V_p [cm^3/g]	d_p [nm]
Biochar top-outlet	2.9 ± 0.3	6.7 ± 0.2	2.8 ± 0.2	33283 ± 211	91.1 ± 0.5	2.1 ± 0.1	0.6 ± 0.1	6.2 ± 0.7	2.85	0.007	3.97
Biochar bottom-outlet	5.1 ± 0.5	13.2 ± 0.3	2.9 ± 0.2	32290 ± 146	87.3 ± 0.9	2.5 ± 0.1	0.5 ± 0.1	9.7 ± 1.1	4.010	0.006	3.97

Moisture, volatiles, ashes, C, H, N, O all in wt%.

- For the exergy analysis of the process, all products are considered useful or valuable, meaning none are regarded as waste.
- In pyrolysis experiments N_2 were used as gas carrier, but it is no taken into account in the calculations.
- For Case C with heat recovery the maximum preheating temperature of biomass was limited to 200 °C, since higher values could trigger premature pyrolysis reactions. The maximum preheating temperature of the combustion air was set to 400 °C, considering material constraints and to avoid operational issues associated with excessively hot inlet streams.
- Kinetic and potential exergy terms are assumed to be negligible.

Additional assumptions are provided in the description of the energy and exergy balances to facilitate understanding.

2.5. Energy balance

The procedure followed in this study is outlined below. The system boundaries adopted for the energy balance calculations correspond to the control volumes defined for each operating case in Figs. 3-6. The

Table 5
Main compounds identified in the OAP of bio-oil by GC–MS.

Compound	Area (%)
Acetone	17.5
Acetic acid	17.2
Phenol	10.8
p-cresol	8.6
2-Butanone	5.5
2-Methylphenol	4.5
Propanoic acid	3.1
Acetol	2.6
3-Furanmethanol	2.2
Furfural	2.0

energy required for the process ($Q_{process}$) to be supplied externally was calculated as the difference between the enthalpy of the output streams (h_{output}) and the input streams (h_{input}) and taken into account the losses of the system (Q_{loss}), see Eq. (1). For Case A and B, h_{output} is the enthalpy of the pyrolysis products, while for Case C is the enthalpy of the biochar and liquids from the pyrolysis and the heat produced in the combustion of the pyrogases in the combustion process (h_{comb}). Additionally, in Case A, the heat associated with cooling the products to the reference state is implicitly assumed to be fully recovered and therefore not treated as an external loss.

$$Q_{process} = h_{output} - h_{input} + Q_{loss} \quad (1)$$

where:

$Q_{process}$: enthalpy required to be supplied externally to the process in MJ•kg^{-1}.

h_{input}: enthalpy of the reactants entering the volume control in MJ•kg^{-1}.

h_{output}: enthalpy of the products leaving the volume control in MJ•kg^{-1}.

Q_{loss}: enthalpy of the process losses in MJ•kg^{-1}.

2.5.1. Enthalpy calculation

The only input of energy considered as an entering to the volume control is the biomass. On the other hand, the considered outlets of the system are the products of the pyrolysis (biochar, bio-oil and pyrogases) for Cases A and B, while in Case C since pyrogases are burned in a combustion chamber the products that go out of the system are steam, CO_2, N_2 and the excess O_2 from the combustion.

The enthalpy of the inlet can be calculated using Eq. (2).

$$h_{input} = \Delta h^0_{f,biomass} \quad (2)$$

where:

$\Delta h^0_{f,biomass}$: standard enthalpy formation of the biomass in MJ•kg^{-1}.

The calculation of the standard formation enthalpies required for the evaluation of h_{input} is described in detail in Section 2.5.2 and expressed through Eq. (13).

The enthalpy of the output products (h_{output}) is calculated for Case A and B using Eq. (3).

$$h_{output} = h_{biochar} + h_{bio-oil} + h_{pyrogases} \quad (3)$$

For Case C, the enthalpy of the products (h_{output}) is calculated by Eq. (4).

$$h_{output} = h_{biochar} + h_{bio-oil} + h_{pyrogases} \quad (4)$$

The overall energetic yield of the process is calculated using Eq. (5).

$$\eta = \left(\frac{\sum h_{output}}{\sum h_{input}}\right) \bullet 100 \quad (5)$$

For Case A, when biomass and the pyrolysis products are considered to be at standard reference state, which means that the heat of the product is being recovered, h_{output} can be calculated as Eq. (6).

$$h_{output} = \frac{\sum_i y_i \bullet \Delta h^0_{f,i}}{100} \quad (6)$$

where:

i: subscript refers to biochar, bio-oil and pyrogases.

y_i: mass fraction yield of the product i, expressed as wt.%.

$\Delta h^0_{f,i}$: standard enthalpy formation for product i, MJ•kg^{-1}.

In Case B and C, products leave the system at the process conditions. Pyrolysis conditions for all the products in Case B, and pyrolysis conditions for biochar and bio-oil and combustion conditions for the products of the oxidation of the pyrogases in Case C. In this scenarios, enthalpies are calculated as it follows.

The $h_{biochar}$ was calculates by Eq. (7).

$$h_{biochar} = \frac{y_{biochar} \bullet (\Delta h^0_{f,biochar} + Cp_{biochar} \bullet (T_{pyr} - T_0))}{100} \quad (7)$$

where:

$Cp_{biochar}$: specific heat capacity of the biochar, calculated using the Hurst-Harrison method, expressed in MJ•kg^{-1}K^{-1}.

The procedure for the calculation of the enthalpy of the bio-oil (liquid fraction) it was developed following the next assumptions. Bio-oil obtained in experiments has two phases, one which is denominated as aqueous phase (AP) and other which is heavier, denominated as heavy phase (HP). Both phases have water in its composition, being the water quantity higher in the first phase mentioned. The quantity of water was determined by Karl-Fischer analysis and the main organic compounds of every phase were determined by GC–MS. For the calculation of the enthalpy of the bio-oil, this fraction was divided in three streams. Water, which is the sum of the water in the AP and in the HP; the organics compounds of the AP (OAP) and the organic compounds of the heavy phase (OHP).

$$h_{bio-oil} = \frac{\sum_j y_j \bullet h_j}{100} \quad (8)$$

where:

j: subscript refers to the water in the bio-oil, AP and HP.

y_j: yield of the product j, expressed as wt.%.

h_j: enthalpy of the product j, MJ•kg^{-1}. This term is calculated using equation for water (9) and (10) for AP and HP.

$$h_j = \frac{y_j}{100} \bullet \left(\Delta h^0_{f,H2O(v)} + \int_{T_0}^{T_{pyr}} Cp_{H2O(v)}(T) \bullet dT\right) \quad (9)$$

where:

y_j: mass fraction yield of water, result of the sum of the content of water in AP and HP, expressed as wt.%.

$\Delta h^0_{f,H2O(v)}$: standard enthalpy formation of the steam j, expressed in MJ•kg^{-1}.

$Cp_{H2O(v)}$: specific heat capacity of the steam, expressed in MJ•kg^{-1}K^{-1}.

$$h_j = \frac{y_j}{100} \bullet \sum_k y_k \bullet \left(\Delta h^0_{f,k} + \int_{T_0}^{T_{pyr}} Cp_k(T) \bullet dT\right) \quad (10)$$

where:

y_j: mass fraction yield of the AP or HP, expressed as wt.%.

k: subscript refers to the organic compounds that form the AP (OAP) and HP (OHP) respectively.

$\Delta h^0_{f,k}$: standard enthalpy formation of organic compound k, expressed in MJ•kg^{-1}.

$Cp_k(T)$: specific heat capacity of organic compound k, expressed in

$MJ \bullet kg^{-1}K^{-1}$.

The $h_{pyrogases}$ was calculated by Eq. (11).

$$h_{pyrogases} = \frac{y_{pyrogases}}{100} \bullet \sum_l y_l \bullet \left(\Delta h^0_{f,l} + \int_{T_0}^{T_{pyr}} Cp_l(T) \bullet dT \right) \quad (11)$$

where:

l: subscript refers to the species that conform the pyrogases. These species are: H_2, N_2, CH_4, CO, CO_2, C_2H_2, C_2H_4 and C_2H_6.

y_l: yield of the specie of the product l, expressed as wt.%.

$\Delta h^0_{f,l}$: standard enthalpy formation of compounds l, expressed in $MJ \bullet kg^{-1}$.

$Cp_l(T)$: specific heat capacity of compound l, expressed in $MJ \bullet kg^{-1}K^{-1}$.

In Case C, is necessary to calculate the enthalpy of the combustion process. Pyrogases are considered to be cooled and enters into the combustion chamber at standard reference state. Enthalpy of the combustion process is calculated by Eq. (12).

$$h_{comb} = \sum_l \Delta h^0_{comb,l} \bullet m_l + \sum_m m_m \bullet \left(\int_{T_0}^{T_{comb}} Cp_m(T) \bullet dT \right) \quad (12)$$

where:

$\Delta h^0_{comb,l}$: combustion enthalpy of compounds l, expressed in $MJ \bullet kg^{-1}$.

m_l: mass of the species l, expressed as kg.

m: subscript refers to the species that appeared after the complete combustion of the pyrogases. These species are: CO_2, steam, N_2 and O_2.

m_m: mass of the specie m, expressed as kg.

$Cp_m(T)$: specific heat capacity of species m, expressed in $MJ \bullet kg^{-1}K^{-1}$.

2.5.2. Standard enthalpy of formation calculation

Standard enthalpies of formation (Δh^0_f) were calculated as described below. The enthalpy formation of solids (biomass and biochar) is calculated by Eq. (13), applying the Hess law. Using the ultimate analysis and higher heating values of biomass and biochar experimentally determined, the Δh^0_f can be calculated with the HHV of the solids and the data of the gases obtained from the combustion of the compounds of biomass and biochar (C, H, N, O, S).

$$\Delta h^0_{f,s} = HHV_s + \sum_n y_n \bullet \Delta h^0_{f,n} \quad (13)$$

where:

s: subscripts refers to solids (biomass and biochar).

HHV_s: higher heating value of the solids (biomass or biochar) in $MJ \bullet kg^{-1}$.

n: indicate the combustion products derived from the elements present in the solid (C, H, O, N, S), which include CO_2, CO, H_2O, NO and SO_2.

y_n: yield of the species of the product n determined by ultimate analysis, expressed as wt.%.

$\Delta h^0_{f,n}$: standard enthalpy formation of species n, expressed in $MJ \bullet kg^{-1}$.

For liquids, the Δh^0_f was calculated with the enthalpy formation of water for the WAP and WOP and using the model compounds that forms the AP and HP (subscript k) and with its mass fraction yields. For the pyrogases, the Δh^0_f was calculated following the same procedure than for the organic liquids fraction, but using the species detected by chromatography (subscript l). The values of Δh^0_f were taken in the reference state since in Case A the products outlet is at the standard reference state [34]. For Case B and C, the outlet state of the compounds is gas and the Δh^0_f was calculated using the coefficients and formulas for thermodynamics properties developed by NASA [35].

Is needed to indicate that for AP the ultimate and proximate analysis were performed but it was impossible to determinate the HHV due to its high water content. However, for HP, proximate, ultimate analysis and HHV were performed. To ensure consistency in both fractions and to carry out the calculations using the same procedure, it was decided to work with the previously mentioned model compounds.

2.5.3. Specific heat capacity calculation

For solids (biomass and biochar), there are no reliable prediction methods for solid heat capacity as function of temperature. The atomic element contribution method of Hurst-Harrison, which is a modification of Kopp's Rule provides estimation at 298.15 K [33]. For Case A, is not necessary to calculate due to products are at the same temperature as the reactive (biomass) entrance. For Cases B and C, *Cp(T)* is evaluated from the reference state (T_0) to the pyrolysis temperature (T_{pyr}) or the combustion temperature (T_{comb}), depending on the compound state. Database of the NASA coefficients for thermodynamic properties were used again [35].

2.6. Exergy balance

The exergy balance for the system of the three study cases is calculated by Eq. (14). The same system boundaries defined for the energy balance, corresponding to the control volumes shown in Figs. 3-6 are adopted for the exergy balance calculations. All exergy calculations are referred to the environmental dead state, defined by a temperature of 298.15 K and a pressure of 1 atm. Exergy losses have been taken into account and are the heat released to the surroundings and the irreversibilities in the process [38]. Exergy is considered to be comprised of physical and chemical exergies, since kinetic and potential exergies are negligible [39], see Eq. (15).

$$\sum e_{input} = \sum e_{output} + \sum e_{loss} \quad (14)$$

where:

e_{input}: exergy of the input streams in $MJ \bullet kg^{-1}$.

e_{output}: exergy of the output streams in $MJ \bullet kg^{-1}$.

e_{loss}: exergy of the losses in $MJ \bullet kg^{-1}$.

$$e = e_{ph} + e_{ch} \quad (15)$$

where:

e_{ph}: physical exergy in $MJ \bullet kg^{-1}$.

e_{ch}: chemical exergy in $MJ \bullet kg^{-1}$.

The input exergy (e_{input}) consists of two components: the exergy of the biomass, which includes both physical and chemical exergy, and the exergy associated with the heat required to carry out the process (e_Q), this exergy can be calculated using Eq. (16).

$$e_Q = Q_{process} \bullet \left(1 - \frac{T_0}{T_{pyr}} \right) \quad (16)$$

where:

e_Q: thermal exergy associated to the needed heat for the process in $MJ \bullet kg^{-1}$.

The exergetic efficiency of the process can be determined through the application of Eq. (17), which relates the useful exergy output to the total exergy input. This efficiency metric provides a quantitative measure of how effectively the available energy is utilized within the system.

$$\psi = \left(\frac{\sum e_{output}}{\sum e_{input}} \right) \bullet 100 \quad (17)$$

2.6.1. Physical exergy calculation

Physical exergy is needed to be taken into account when the products are at different conditions that the biomass (inlet to the system) which is at reference state. The physical exergy can be calculated with Eq. (18). This Eq. consists of two terms, which can be further decomposed in Eq. (19) and Eq. (20), respectively.

$$e_{ph,i} = (h_i - h_{0,i}) - T_0 \bullet (s_i - s_{0,i}) \quad (18)$$

where:

$e_{ph,i}$: physical exergy of the product i, expressed in MJ•kg^{-1}.

h_i: enthalpy of the product i in MJ•kg^{-1}.

$h_{0,i}$: enthalpy of the product i at the standard conditions, in MJ•kg^{-1}.

s_i: entropy of the product i in MJ•kg^{-1}.

$s_{0,i}$: entropy of the product i at the standard conditions, in MJ•kg^{-1}.

$$h_i - h_{0,i} = \int_{T_0}^{T} Cp(T) \bullet dT \quad (19)$$

$$s_i - s_{0,i} = \int_{T_0}^{T} \frac{Cp(T)}{T} \bullet dT - R \bullet ln\left(\frac{P}{P_0}\right) \quad (20)$$

where:

R: is the universal gas constant, with a value of 8.314 J·mol^{-1}·K^{-1}.

P: process, pressure in Pa.

P_0: pressure at reference state, 1.01•10^5 Pa.

(20) can be approximated as zero. With this assumption, Eq. (18) can be equivalently expressed in the form of Eq. (21).

$$e_{ph,i} = \int_{T_0}^{T} Cp(T) \bullet dT - T_0 \bullet \int_{T_0}^{T} \frac{Cp(T)}{T} \bullet dT \quad (21)$$

For solids (biomass and biochar), e_{ph} can be directly calculated using Eq. (21), as all the terms are known and have been described during the explanation of the energy balance. Moreover, this value (e_{ph}) is typically small compared to the corresponding chemical exergy.

Since the values of s and s_0 are obtained from the NASA database [35], physical exergy calculation for liquids phases (water, AP and HP) can be calculated as it follows. Eq. (22) for water fraction and Eq. (23) for AP and HP.

$$e_{ph,j} = \frac{y_j}{100} \bullet \left(\int_{T_0}^{T_{pyr}} Cp_{H2O(v)}(T) \bullet dT - T_0 \bullet \int_{T_0}^{T} \frac{Cp_{H2O(v)}(T)}{T} \bullet dT \right) \quad (22)$$

$$e_{ph,j} = \frac{y_j}{100} \bullet \sum_k y_k \left(\int_{T_0}^{T_{pyr}} Cp_k(T) \bullet dT - T_0 \bullet \int_{T_0}^{T} \frac{Cp_k(T)}{T} \bullet dT \right) \quad (23)$$

where:

$e_{ph,j}$: physical exergy of the compound j, in MJ•kg^{-1}.

For the pyrogases, e_{ph} can be calculated by Eq. (24), which follows the same procedure that for the calculation of the organic phases of the bio-oil.

$$e_{ph,l} = \frac{y_{pyrogases}}{100} \bullet \sum_l y_l \left(\int_{T_0}^{T_{pyr}} Cp_l(T) \bullet dT - T_0 \bullet \int_{T_0}^{T} \frac{Cp_l(T)}{T} \bullet dT \right) \quad (24)$$

where:

$e_{ph,l}$: physical exergy of the compound l, in MJ•kg^{-1}.

2.6.2. Chemical exergy calculation

Chemical exergy of biomass and products is calculated based on their elemental composition and standard chemical exergy values of reference species. If the feedstock and all resulting products are considered to be at standard reference temperature and pressure, the exergy is reduced to its chemical component, which represents the exergy of a compound in the standard reference state. For the liquid fraction (water, AP, and HP) and the pyrogases, the chemical exergy values (e_{ch}) of all constituent species can be obtained from the literature [39]. On the other hand, to estimate the e_{ch} of the biomass and biochar is challenging since these phases are composed of multiple compounds. Various correlations exist for estimating the chemical exergy of both liquid and solid fuels. As previously mentioned, the chemical exergy of bio-oil can be determined based on its known chemical constituents. In contrast, for fossil fuels (biomass and biochar) empirical correlations proposed by Szargut et al. [39], which are based on the lower heating value (LHV) and specific exergy coefficients, are commonly used. Other studies propose estimations for biomass exergy like Hepbasli [40], Shieh and Fan [41] or Rao et al. [42]. Kaushik and Singh proposed a method for the estimation of chemical exergy for solids fuels with moisture and a negligible content of sulfur and ash [43]. This last method has been chosen for the e_{ch} calculation of biomass and biochar since their elemental composition is comparable to that of solid fossil fuels. Therefore, correlations developed for solid fossil fuels, such as those proposed by Szargut et al. [39],are frequently applied for estimating their chemical exergy.

Chemical exergy for biomass or biochar can be calculated by Eq. (25).

$$e_{ch,solid} = \left((LHV_{solid} + \lambda \bullet y_{moist}) \bullet \varphi_{db} + 9417 \bullet y_{S,db} \right) \bullet \frac{1}{1000} \quad (25)$$

where:

$e_{ch,solid}$: chemical exergy of the solid (biomass or biochar), in MJ•kg^{-1}.

LHV_{solid}: lower heating value of the solid, in kJ•kg^{-1}.

λ: latent heat of vaporization of water at standard reference state. 2442 kJ•kg^{-1}.

y_{moist}: mass fraction of moisture in the solid, determined by proximate analysis in wt.%.

φ_{db}: ratio of standard specific chemical exergy to the net calorific value. Described by Eq. (26).

$y_{S,db}$: mass fraction of sulfur in dry basis, determined by ultimate analysis in wt.%.

As can be seen in Table 1 the content in sulfur is negligible in biomass, and consequently, it is also negligible in the resulting biochar, therefore the second term on Eq. (25) is considered zero.

$$\varphi_{db} = 1.0437 + 0.1882 \bullet \frac{y_{H,db}}{y_{C,db}} + 0.0610 \bullet \frac{y_{O,db}}{y_{C,db}} + 0.0404 \bullet \frac{y_{N,db}}{y_{C,db}} \quad (26)$$

where:

$y_{element,db}$: mass fraction of the element on a dry basis, determined by ultimate analysis and expressed as wt.%.

Chemical exergy of liquid fraction (water, AP or HP) can be calculated as it follows. Eq. (27) for water fraction and Eq. (28) for AP and HP.

$$e_{ch,j} = \frac{y_j}{100} \bullet e_{ch,water} \quad (27)$$

$$e_{ch,j} = \frac{y_j}{100} \bullet \sum_k y_k \bullet e_{ch,k} \quad (28)$$

where:

$e_{ch,j}$: chemical exergy of the compound j in MJ•kg^{-1}.

$e_{ch,water}$: chemical exergy of the water in MJ•kg^{-1}.

$e_{ch,k}$: chemical exergy of the compound k in MJ•kg^{-1}.

Chemical exergy of the pyrogases, e_{ch} can be calculated by Eq. (29).

$$e_{ch,l} = \frac{y_{pyrogases}}{100} \bullet \sum_k y_l \bullet e_{ch,l} \quad (29)$$

where:

$e_{ch,l}$: chemical exergy of the compound l, in MJ•kg^{-1}.

3. Results

All experimental cases were performed using the same biomass feedstock; as a result, variations in feedstock composition do not affect the comparative analysis between configurations. The elemental composition and heating value of the biomass mainly affect the calculated energy input and chemical exergy, influencing the absolute values of the performance indicators, while the comparative trends between operating cases remain unaffected.

3.1. Pyrolysis experimental results

The experimental mass balance results for both outlet configurations are summarized in Table 3. On average, the char yield was slightly higher for the bottom outlet (33.7 wt%) compared to the top outlet (30.5 wt%), whereas the production of liquids showed the opposite trend, increasing from 27.5 wt% in the bottom configuration to 29.9 wt % in the top configuration. Gas yields remained similar in both cases, although a small increase was observed for the top outlet (39.6 wt% vs. 38.8 wt%). These differences can be attributed to the different gas flow patterns inside the reactor. In the top configuration, vapors and gases are evacuated more rapidly, which reduces secondary condensation and repolymerization phenomena on the char surface. Product distribution results are similar to other studies of biomass pyrolysis [32,44]. As a consequence, char is obtained with lower volatile content and reduced moisture retention, while a slightly higher fraction of bio-oil is collected. Similar effects have been reported in fixed-bed pyrolysis studies, where vapor residence time plays a critical role in determining the final product distribution [45–47].

Regarding the gas composition, the top outlet configuration resulted in a higher fraction of H_2 (27.4 vol% vs. 22.8 vol%), as well as increased C_2 species, particularly ethylene (1.7 vol% vs. 0.6 vol%). In contrast, CO content decreased slightly in the top configuration (16.3 vol% vs. 17.5 vol%). These shifts in composition are consistent with enhanced cracking reactions and reduced secondary condensation when gases are swiftly removed from the hot char matrix. As a result, the calorific value of the gas mixture was significantly improved. When expressed per unit mass of biomass, the LHV of the syngas averaged 4.8 MJ/$kg_{biomass}$ for the top outlet and 4.1 MJ/$kg_{biomass}$ for the bottom outlet. In this case, the difference is moderate, as the error bars partially overlap. However, when expressed on a volumetric basis, the contrast becomes more pronounced: 12.2 MJ/m^3(STP) for the top outlet versus 11.3 MJ/m^3(STP) for the bottom outlet. These results confirm that the top outlet configuration favors the production of higher-quality syngas, particularly in terms of energy density per unit volume. The values observed in this work (12.2 MJ/m^3 for the top outlet and 11.3 MJ/m^3 for the bottom outlet) fall within the range reported in the literature for pyrolysis and gasification in fixed-bed systems. For instance, Cong et al. documented LHVs between 6 and 17 MJ/m^3 in different slow pyrolysis setups [48], with significant improvements when oxygen was used as the oxidizing agent. Moreover, reviews on fixed-bed technology cite a common range of 4–15 MJ/m^3, which is consistent with the results obtained in this study [49].

These findings are consistent with results reported for biomass pyrolysis in fixed-bed and downdraft reactors, where gas residence time has been identified as a crucial factor influencing product distribution and syngas quality. Vieira et al. showed that shorter vapor residence times favor the release of lighter gases and increase the heating value of syngas [47], while Tabal et al. reported that prolonged percolation through the char layer enhances re-condensation and tar formation, reducing gas quality [46]. In the present study, the superior performance of the top outlet can be attributed to the minimization of these effects, as volatiles are evacuated more rapidly and avoid re-contact with the char bed. Consequently, the top outlet not only improved bio-oil recovery but also enhanced the calorific value of the gas fraction, making it more suitable for energetic valorization. Although the bottom outlet produced slightly more char, this fraction was richer in volatiles, reducing its energy density and stability. Overall, these results emphasize the importance of reactor design and outlet configuration in optimizing slow pyrolysis, in agreement with previous studies that highlight the key role of hydrodynamics and vapor residence time [46,47,49]. Similar conclusions were drawn by Bridgwater [50] for fast pyrolysis, confirming that vapor residence time is a universal factor determining yields and quality across pyrolysis regimes.

Additionally, in the last column of Table 3 are summarized the results of the long experiment performed with the top outlet configuration. The aim of this experiment is to check the results observed in a longer experiment. As can be observed all the results of the mass balance and the gas properties are inside the static deviation presented by the experiments with top outlet configuration. This indicates that the system exhibits similar behavior over longer periods of operation.

3.1.1. Characterization of biochar

The characterization of the biochar obtained from the two outlet configurations is summarized in Table 4. Clear differences were observed between the samples. The biochar from the bottom outlet showed higher moisture (5.1 wt%) and volatile matter (13.2 wt%) compared to the top outlet (2.9 wt% and 6.7 wt%, respectively). This indicates partial condensation of vapors in the char when gases exit through the lower part of the reactor, as also reflected in the strong odor of organic compounds detected in these samples.

In contrast, the top-outlet char exhibited a higher fixed carbon content (91.1 wt%) and a slightly higher lower heating value (33.3 MJ/kg) than the bottom-outlet char (87.3 wt% C, 32.3 MJ/kg). This composition is consistent with typical ranges reported for slow pyrolysis biochar, where carbon contents between 76–90 wt% are common [51], and also in line with values reported for lignocellulosic chars, which generally show 80–90 wt% C with BET surface areas below 10 m^2/g under slow pyrolysis conditions [52].

Regarding textural properties, BET analysis revealed a larger surface area for the bottom-outlet char (4.10 m^2/g) compared to the top-outlet char (2.85 m^2/g), although pore volume and average diameter remained similar. This suggests that while the top configuration favors the production of a more carbon-rich and stable char, the bottom configuration enhances surface development, which could be relevant for adsorption-oriented applications.

Overall, the results highlight that the top outlet configuration leads to a higher-quality char for energy and soil amendment purposes, while the bottom outlet may be advantageous if surface area is prioritized. In addition, maintaining biochar as a stable carbon sink links its valorization to the generation of CO_2 Removal Certificates (CORCs), reinforcing both the environmental and economic relevance of this product.

3.1.2. Characterization of pyrolysis liquids

The OAP of the bio-oil was first evaluated in terms of its water content, and the Karl Fischer titration revealed that the sample contained 84.2 wt% water, confirming the highly aqueous character of this phase. The compositional analysis by GC–MS allowed the identification of the main compounds and their relative abundance, which are presented in Table 5. The most prominent components were acetone, acetic acid, phenol, and p-cresol, along with minor contributions from 2-butanone, 2-methylphenol, and propanoic acid. For subsequent calculations, the identified compounds were grouped into three main chemical families: carboxylic acids, ketones, and phenolic compounds. To simplify the analysis and ensure comparability, each family was considered to contribute equally of the organic fraction (33%).

The elemental composition and energy content of the OHP of bio-oil are summarized in Table 6, where the results are presented separately for the bio-oil obtained with the upper gas outlet configuration and with the lower gas outlet configuration. A marked difference was observed between the two cases. In the upper gas outlet, the organic fraction exhibited a high carbon content (73.9 wt%) and a relatively lower hydrogen content, resulting in a higher lower heating value (LHV) of

Table 6
Elemental composition and LHV of the OHP of bio-oil in both configurations.

	C (wt. %)	H (wt. %)	N (wt. %)	LHV [kJ/kg]
OHP top outlet configuration	73.9	8.1	0.37	31,829
OHP bottom outlet configuration	38.7	14.5	–	21,984

approximately 32 MJ/kg. In contrast, the lower gas outlet configuration led to a significant decrease in carbon content (38.7 wt%) accompanied by an increase in hydrogen content (14.5 wt%), which was reflected in a substantially lower LHV of around 22 MJ/kg. These differences highlight the strong influence of reactor configuration on both the composition and the energetic quality of the organic fraction. Water content determined by Karl Fischer revealed a contnen of 8–10 wt% in OHP for bottom outlet configuration and 4–5 wt% for top outlet configuration. Additionally, Table 7 shows the compositional analysis by GC–MS which allowed the identification of the main compounds and their relative abundance.

3.2. Energy balance results

The energy results for every experiment and case are shown in Table 8. In all scenarios analyzed, the pyrolysis process exhibited an endothermic character, although the magnitude of $Q_{process}$ was highly dependent on the operating configuration and the extent of energy integration. As part of the energy balance calculations, the standard formation enthalpy of the biomass feedstock was determined following the procedure described in Eq. (13), yielding a value of –6.6 MJ/kg. For biochar, the calculated standard formation enthalpy depends on the outlet configuration, resulting in values of 0.5 MJ/kg for the top outlet and 0.2 MJ/kg for the bottom outlet. These values are subsequently used as input data for the energy and exergy balance results discussed in this section. When only the pyrolysis process was considered without any further integration (Case A), the required heat ranged from 1.18 to 1.58 MJ/kg, with efficiencies between 77% and 83%. These values are in agreement with previous studies of slow pyrolysis of lignocellulosic biomass, which typically reported heat demands of 1.0 to 1.5 MJ/kg under similar operating conditions [11,32,45,53]. Within this scenario, slightly higher efficiencies were observed when the gas outlet was located at the top of the reactor. This suggests that hydrodynamic conditions play a relevant role in improving heat transfer and reducing energy demand, consistent with the findings of Peters et al. [54], who highlighted the influence of flow configuration on thermal gradients and product distribution in fast pyrolysis reactors. Observed heat demand aligns well with values reported for slow pyrolysis, over 1.0–1.5 MJ/kg [11,32].

In contrast, Case B considered that products leave the system at the pyrolysis temperature (600 °C), with no recovery of sensible or latent heat. Under these conditions, the process requirements nearly doubled, reaching values close to 3 MJ/kg, while efficiencies decreased to values over 60%. This behavior is consistent with the literature [53,55] which shows that increased reaction severity—associated with enhanced devolatilization and secondary cracking—leads to higher endothermicity. Such results underline the strong sensitivity of $Q_{process}$ to energy recovery assumptions: while under mild operation pyrolysis can be nearly thermoneutral, the process becomes strongly endothermic when products are not cooled to the reference state.

When the combustion of pyrolysis gases was included (Case C without heat recovery), the external heat requirement decreased to values comparable to Case A, with Qprocess ranging between 1.0 and 1.6 MJ/kg depending on the outlet configuration. In the top-outlet configuration, efficiencies above 90% were reached, highlighting the strong contribution of pyrolysis gas combustion to sustaining the process. This strategy is consistent with experiences reported at pilot and commercial scale: Pilot-scale experience also points in this direction. For instance, IEA Bioenergy reported in a Task 34 technical note the transition of pilot units into a second phase where non-condensable gases were robustly reused as process heat, while their 2022 state-of-the-art review shows that several commercial pyrolysis plants already combust both char and non-condensable gases (pyrogases in this work) to cover the full thermal demand of the process [56]. Autothermal operation has also been validated experimentally: Polin [57] demonstrated that replacing N_2 with air in a fluidized bed enables the oxidation of internal streams to meet the heat requirements, and Chavando et al. [58] simulated continuous reactors where char and gases serve as energy carriers to sustain operation. More recently, Cavalloni et al. [59] confirmed that oxidative pyrolysis with sub-stoichiometric air can replace external heat input while simplifying reactor design. Industrial integration examples also support this concept: Amari et al. [60] described a sewage sludge carbonization system where pyrolysis gases are combusted and the resulting heat is recovered to preheat combustion air and other process streams, thereby reducing fossil energy demand. Experimental evidence supports that autothermal operation via combustion of pyrolysis vapors—without involving char—can adequately meet the heat demand. Milhé et al. [61] demonstrated this in a continuous fixed-bed reactor with air injection, where internal oxidation sustains the process while maintaining char yield. This aligns well with the observations for Case C: high efficiencies achieved in the top-outlet configuration are consistent with such autothermal behavior.

Nevertheless, in the framework of slow pyrolysis, char is not considered as a fuel but rather as a value-added product intended for agricultural use and carbon sequestration. Its valorization as biochar is directly linked to the generation of CO_2 Removal Certificates (CORCs), which provide both economic incentives and climate benefits by maintaining char as a long-term carbon sink [62,63]. For this reason, in the present study only the combustion of pyrogases gases was considered, ensuring that biochar remains available for applications that maximize its agronomic and environmental value.

When both combustion and heat recovery were integrated (Case C with heat recovery), the external heat demand dropped drastically-down to as low as 0.10 MJ/kg in the top-outlet configuration. In some runs, slightly negative values even emerged, indicating that the recovered exhaust-gas energy could exceed the process needs, pushing the effective efficiency to—or even above—100%, a behavior that mirrors a quasi-autothermal regime. This level of integration has been validated in the literature: Polin et al. demonstrated that partial oxidation of volatiles in a fluidized-bed fast pyrolysis reactor could fully satisfy the thermal demand, achieving autothermal operation [57]. Similarly, Islam et al. quantified that heat recovery in integrated biomass-to-syngas systems reduces external energy input by 30–40% [64]. Brown further emphasizes that coupling exothermic and endothermic reactions allows direct thermal balancing within the process [65], while Huang et al. highlights how oxidative/autothermal pyrolysis systems can be designed to eliminate the need for external heat altogether [66]. These studies provide solid benchmarks for comparison and contextualize the excellent energy performance observed under optimal integration in the present work. In addition, Table 9 shows the energy results for the long experiment performed. These results fall within the static deviation presented by the experiments with top outlet configuration, indicating that the system behavior is the same under longer time ranges, as was the case with mass balance.

In summary, the comparison between scenarios shows that direct pyrolysis without energy recovery (Case B) represents the most energy-demanding configuration, requiring close to 3 MJ/kg. Conventional

Table 7
Main compounds identified in the OHP of bio-oil by GC–MS.

Compound	Area (%)
3-Methylphenol	16.0
2-Methylphenol	13.0
Phenol	11.3
3-Ethylphenol	8.0
Naphtalene	7.3
3,5-Dimethylphenol	7.2
Indene	5.7
1,3-Dimethylbenzene	6.7
2-Methylnaphtalene	3.6
1-Propynylbenzene	2.4

Table 8
Energy balance results of the experiments performed.

	Case A							
	Bot. 1	Bot. 2	Bot. 3	Av. Bot.	Top 1	Top 2	Top 3	Av. Top
$Q_{process}$ [MJ/kg]	1.58	1.34	1.18	1.37 ± 0.20	1.30	1.19	1.25	1.25 ± 0.06
η [%]	77.34	80.69	83.03	80.35 ± 2.86	81.28	82.98	82.08	82.11 ± 0.85
	Case B							
	Bot. 1	Bot. 2	Bot. 3	Av. Bot.	Top 1	Top 2	Top 3	Av. Top
$Q_{process}$ [MJ/kg]	2.97	2.75	2.59	2.77 ± 0.19	2.76	2.64	2.74	2.71 ± 0.06
η [%]	57.33	60.51	62.74	60.19 ± 2.72	60.40	62.13	60.71	61.08 ± 0.92
	Case C without heat recovery							
	Bot. 1	Bot. 2	Bot. 3	Av. Bot.	Top 1	Top 2	Top 3	Av. Top
$Q_{process}$ [MJ/ kg]	1.64	1.84	1.35	1.61 ± 0.25	1.39	0.60	0.94	0.98 ± 0.40
η [%]	76.81	73.98	80.95	77.25 ± 3.51	80.33	90.44	86.73	85.83 ± 5.11
	Case C with heat recovery							
	Bot. 1	Bot. 2	Bot. 3	Av. Bot.	Top 1	Top 2	Top 3	Av. Top
$Q_{process}$ [MJ/ kg]	0.87	1.09	0.51	0.82 ± 0.29	0.57	−0.34	0.07	0.10 ± 0.46
η [%]	87.75	84.62	92.78	88.38 ± 4.12	91.93	104.91	99.08	98.64 ± 6.50

Table 9
Energy balance results of the long experiment performed.

	Case A	Case B	Case C without heat recovery	Case C with heat recovery
$Q_{process}$ [MJ/ kg]	1.30	2.77	1.05	0.20
η [%]	81.28	60.24	85.12	97.23

pyrolysis with recovery (Case A) lowers this demand to around 1.3 MJ/kg, but the integration of combustion and heat recovery (Case C) nearly eliminates the external heat requirement. This demonstrates the strong potential of energy integration strategies to enhance the thermal performance of biomass pyrolysis, reducing external energy dependence and moving the process closer to practical autothermal operation.

3.3. Exergy balance results

Table 10 summarizes the exergy balance results of the experiments performed. For Case A, no values of $e_{process}$ or exergy efficiency (ψ) are reported, since all products were assumed to leave the system at the reference state (25 °C, 1 atm). Under these conditions, the physical exergy of the product streams vanishes and only the chemical exergy remains. This scenario is primarily theoretical and serves as a benchmark, as no process exergy demand is explicitly assigned.

In Case B, where products were considered at the pyrolysis temperature (600 °C), the process exergy requirement averaged 3.31 ± 0.39 MJ/kg for the bottom outlet and 3.02 ± 0.37 MJ/kg for the top outlet. Corresponding exergy efficiencies were 85.26 ± 1.72% and 86.56 ± 1.65%, respectively. These values are comparable to literature data. Greco et al. reported efficiencies of 55–61% for wheat straw slow pyrolysis [67], noting improvements with higher pressures and shorter vapor residence times. Similarly, Wang et al. reported syngas exergy efficiencies of 52.9–60.6% for rice husk pyrolysis at high temperatures [68]. Atienza-Martínez et al. also documented efficiencies between 72% and 83% for sewage sludge pyrolysis [53]. No significant differences were observed between the top and bottom outlet configurations for the exergy results in this case.

When combustion of pyrogases (Case C) is included, the total exergy demand increases compared with the non-integrated configuration (Case B), since the combustion stage itself is strongly exothermic and involves additional exergy flows and destructions: $e_{process}$ is 5.41 ± 0.43 MJ/kg for the bottom outlet and 5.22 ± 0.48 MJ/kg for the top outlet. The corresponding exergy efficiencies decreased to 75.11 ± 2.16% and 75.51 ± 2.41%, respectively. The comparison between outlet configurations showed in this case no differences in the exergy balance between outlet configurations. Despite this higher exergy throughput, the resulting exergy efficiencies are lower than in Case B because of the different system boundaries and product definitions. In Case B, the stream of pyrogases is treated as a useful product −its chemical exergy can be exploited as fuel or for further upgrading- while in the Case C configurations, the combustion converts this high-quality gas into exhaust gases with much lower exergy content. As a consequence, even though the process becomes more thermally self-sustained, the overall exergy efficiency decreases to values around 75–78%, as summarized in Table 10. The observed decrease in exergy efficiency when pyrolysis gases are combusted is mainly associated with the intrinsic chemical irreversibility of the combustion process, which converts high-quality chemical exergy into low-grade thermal exergy of the exhaust gases. Additional exergy destruction arises from heat transfer across finite

Table 10
Exergy balance results of the experiments performed.

	Case A							
	Bot. 1	Bot. 2	Bot. 3	Av. Bot.	Top 1	Top 2	Top 3	Av. Top
$e_{process}$ [MJ/kg]	–	–	–	–	–	–	–	–
ψ [%]	–	–	–	–	–	–	–	–
	Case B							
	Bot. 1	Bot. 2	Bot. 3	Av. Bot.	Top 1	Top 2	Top 3	Av. Top
$e_{process}$ [MJ/kg]	3.58	2.86	3.50	3.31 ± 0.39	3.07	3.36	2.63	3.02 ± 0.37
ψ [%]	84.17	87.25	84.37	85.26 ± 1.72	86.36	85.02	88.30	86.56 ± 1.65
	Case C without heat recovery							
	Bot. 1	Bot. 2	Bot. 3	Av. Bot.	Top 1	Top 2	Top 3	Av. Top
$e_{process}$ [MJ/kg]	5.50	4.94	5.78	5.41 ± 0.43	5.18	5.71	4.76	5.22 ± 0.48
ψ [%]	74.72	77.44	73.18	75.11 ± 2.16	76.00	72.89	77.64	± 2.41
	Case C with heat recovery							
	Bot. 1	Bot. 2	Bot. 3	Av. Bot.	Top 1	Top 2	Top 3	Av. Top
$e_{process}$ [MJ/kg]	4.99	4.44	5.23	4.89 ± 0.41	4.64	5.09	4.18	4.64 ± 0.46
ψ [%]	76.51	79.23	75.11	76.95 ± 2.09	77.95	75.10	79.79	± 2.36

temperature differences during heat recovery; however, this contribution is secondary compared to the chemical irreversibility of gas combustion. These results are consistent with other integrated approaches. Campusano et al. reported exergy efficiencies of 90.3% for non-catalytic auger pyrolysis and 91.6% for catalytic upgrading at 500 °C [15]. Similarly, Milhé et al. demonstrated autothermal operation in a fixed-bed pyrolysis reactor, validating that partial oxidation of process gases can sustain the thermal requirements [61]. In the context of fast pyrolysis, Boateng et al. reported exergy efficiencies of 52–67% experimentally and up to 94% in simulations, highlighting the strong potential of integration strategies [14]. More recently, exergy analyses of integrated pyrolysis–bioenergy systems have shown that heat recovery can reduce external energy inputs by more than 30% [64].

When heat recovery is also included (Case C with heat recovery), the process exergy demand slightly decreases compared with Case C without heat recovery, since part of the released heat is reused to preheat the incoming air and biomass. However, the overall exergy efficiency only increases marginally because the recovered heat is of lower quality (lower temperature level) and the chemical exergy of the pyrogases is still lost through combustion. As a result, the Case C with heat recovery configuration exhibits ψ values close to 77–78%, slightly higher than Case C without heat recovery but still clearly below those of Case B. This outcome highlights that thermal integration mainly benefits the energy balance rather than the exergy performance.

Overall, the results confirm that Case B is the configuration with the highest exergy efficiency, since the pyrogases stream is considered as a useful product with significant chemical exergy. In contrast, the combustion-based configurations (Cases C), particularly that with heat recovery, move the process toward quasi-autothermal conditions by reducing the external heat demand, but the overall exergy efficiency decreases because the exergy-rich pyrogases are converted into combustion gases with lower quality. These findings are consistent with the observed trends in the literature, emphasizing the trade-off between energetic self-sufficiency and exergy performance in integrated pyrolysis systems.

Furthermore, Table 11 shows the results of the exergy balance for the long experiment. As was the case with the mass and energy balance results, the results agree within the statistical deviation with those obtained in the shorter experiments with the top outlet configuration.

3.4. Reliability and uncertainty considerations

The reliability of the reported energy and exergy balance results is mainly influenced by uncertainties associated with biomass feeding rate, product yield measurements, gas composition analysis, and temperature measurements. While these uncertainties may affect the absolute values of the calculated energy and exergy efficiencies, the comparative trends observed between the different operating cases are considered robust, as all experiments were conducted using the same experimental setup, measurement devices, and data processing methodology. In addition, the observed energy distribution among products and the calculated energy and exergy efficiencies are in line with values reported in the literature for fixed-bed biomass pyrolysis systems operating under comparable conditions.

Table 11
Exergy balance results of the long experiment performed.

	Case A	Case B	Case C without heat recovery	Case C with heat recovery
$e_{process}$ [MJ/kg]	–	2.99	5.07	4.51
ψ [%]	–	86.70	76.23	78.31

4. Conclusions

The present paper provides the methodology for calculating the energy and exergy balances of a biomass pyrolysis pilot plant, as well as the results obtained for different scenarios (pyrolysis without energy recovery, pyrolysis with energy recovery from products, and pyrolysis with combustion of the non-condensable gases coupled with exhaust-gas heat recovery). The methodology proposed allowed a consistent comparison of the results under different operating modes and outlet configurations. The following conclusions can be drawn from the calculations made:

The results showed that the energy demand of pyrolysis strongly depended on the assumptions made for heat recovery. When products were cooled to the reference state, the external heat required was relatively low (≈1.3 MJ/kg). When products were considered at the pyrolysis temperature, the process became nearly twice as endothermic, with heat requirements approaching 3 MJ/kg. Combustion of the pyrolysis gases substantially decreased the heat demand, while integrating exhaust-gas recovery further reduced it, leading in some cases to quasi-autothermal operation.

Exergy analysis showed that although the integration of gas combustion and heat recovery reduces external energy inputs and moves the system toward autothermal operation, it also decreases the overall exergy efficiency compared with the non-integrated configuration. In the base case, where the pyrogases stream is considered a useful product, the exergy efficiency reached values around 86%. When the gases were combusted, the total process exergy demand increased due to the exothermic nature of the reaction, while efficiencies dropped to approximately 75–78%. This outcome reflects the loss of high-quality chemical exergy associated with the conversion of pyrogases into exhaust gases and highlights the trade-off between energy self-sufficiency and exergy performance.

The comparison between gas outlet configurations demonstrated that the top outlet improved product distribution and energy quality. This configuration increased liquid yields and gas calorific value while reducing moisture and volatile content in biochar, leading to a more stable, carbon-rich solid. Consequently, the top outlet combined with gas combustion and heat recovery proved to be the most efficient configuration both energetically and exergetically.

For all scenarios studied, the results of the 10 h continuous experiment confirmed the stability of the system, as mass, energy, and exergy balances remained within the statistical deviation of shorter tests. This provides evidence of robust operation under the optimized configuration.

Overall, the integration of pyrolysis gas combustion and exhaust heat recovery represents a practical strategy to minimize external heat requirements and improve exergy efficiency, while preserving biochar as a carbon-negative product. These findings reinforce the relevance of process integration and hydrodynamic design in advancing the energy and climate performance of biomass pyrolysis systems. From a broader process and sustainability perspective, the combined energy-exergy assessment presented in this work provides a useful basis for guiding energy integration strategies and supporting informed design and operational decisions in biomass pyrolysis systems.

Future work may extend the present analysis to alternative reactor scales, oxidative or autothermal pyrolysis configurations, and the exergy-based evaluation of specific end-use applications of pyrolysis products.

CRediT authorship contribution statement

César Gracia-Monforte: Writing – original draft, Validation, Software, Methodology, Investigation, Formal analysis, Data curation, Conceptualization. **Alejandro Lete:** Writing – review & editing, Methodology, Investigation. **Frédéric Marias:** Writing – review & editing, Validation, Supervision, Conceptualization. **Javier Ábrego:** Writing –

review & editing, Validation, Supervision, Resources, Project administration. **Jesús Arauzo:** Resources, Project administration, Funding acquisition.

Declaration of competing interest

The authors declare that they have no known competing financial interests or personal relationships that could have appeared to influence the work reported in this paper.

Acknowledgments

The authors express gratitude for providing frame support for this work to the Project PID2023-1490520B-I00 funded by Agencia Estatal de Investigación and by the European Union. Aragón Government has also given frame support (Research Group Ref. T22_23R).

Appendix A. Supplementary data

Supplementary data to this article can be found online at https://doi.org/10.1016/j.enconman.2026.121154.

Data availability

Data will be made available on request.

References

[1] Garcia-Nunez JA, Pelaez-Samaniego MR, Garcia-Perez ME, Fonts I, Abrego J, Westerhof RJM, et al. Historical developments of pyrolysis reactors: a review. Energy Fuels 2017;31:5751–75. https://doi.org/10.1021/acs.energyfuels.7b00641.

[2] Mkhize NM, Danon B, Alvarez J, Lopez G, Amutio M, Bilbao J, et al. Influence of reactor and condensation system design on tyre pyrolysis products yields. J Anal Appl Pyrol 2019;143. https://doi.org/10.1016/j.jaap.2019.104683.

[3] Barr MR, Volpe R, Kandiyoti R. Influence of reactor design on product distributions from biomass pyrolysis. ACS Sustain Chem Eng 2019;7:13734–45. https://doi.org/10.1021/acssuschemeng.9b01368.

[4] Talwar P, Agudelo MA, Nanda S. Pyrolysis process, reactors, products, and applications: a review. Energies (Basel) 2025;18. https://doi.org/10.3390/en18112979.

[5] Karvonen J, Kunttu J, Suominen T, Kangas J, Leskinen P, Judl J. Integrating fast pyrolysis reactor with combined heat and power plant improves environmental and energy efficiency in bio-oil production. J Clean Prod 2018;183:143–52. https://doi.org/10.1016/j.jclepro.2018.02.143.

[6] Comendador P, Santamaria L, Amutio M, Alvarez J, Olazar M, Lopez G. Energy analysis and heat integration in the joint process of biomass fast pyrolysis and in line sorption enhanced steam reforming. Energy Fuels 2024;38:14402–13. https://doi.org/10.1021/acs.energyfuels.4c02555.

[7] Yang Y, Brammer JG, Wright DG, Scott JA, Serrano C, Bridgwater AV. Combined heat and power from the intermediate pyrolysis of biomass materials: performance, economics and environmental. Impact 2017.

[8] Crombie K, Mašek O. Investigating the potential for a self-sustaining slow pyrolysis system under varying operating conditions. Bioresour Technol 2014;162:148–56. https://doi.org/10.1016/j.biortech.2014.03.134.

[9] Ábrego J, Atienza-Martínez M, Plou F, Arauzo J. Heat requirement for fixed bed pyrolysis of beechwood chips. Energy 2019;178:145–57. https://doi.org/10.1016/j.energy.2019.04.078.

[10] Cong H, Mašek O, Zhao L, Yao Z, Meng H, Hu E, et al. Slow pyrolysis performance and energy balance of corn stover in continuous pyrolysis-based poly-generation systems. Energy Fuels 2018;32:3743–50. https://doi.org/10.1021/acs.energyfuels.7b03175.

[11] Daugaard DE, Brown RC. Enthalpy for pyrolysis for several types of biomass. Energy Fuels 2003;17:934–9. https://doi.org/10.1021/ef020260x.

[12] Fonts I, Atienza-Martínez M, Carstensen HH, Benés M, Pires APP, Garcia-Perez M, et al. Thermodynamic and physical property estimation of compounds derived from the fast pyrolysis of lignocellulosic materials. Energy Fuels 2021;35:17114–37. https://doi.org/10.1021/acs.energyfuels.1c01709.

[13] Jerzak W, Reinmöller M, Magdziarz A. Estimation of the heat required for intermediate pyrolysis of biomass. Clean Techn Environ Policy 2022;24:3061–75. https://doi.org/10.1007/s10098-022-02391-1.

[14] Boateng AA, Mullen CA, Osgood-Jacobs L, Carlson P, Macken N. Mass balance, energy, and exergy analysis of bio-oil production by fast pyrolysis. J Energy Res Technol 2012;134. https://doi.org/10.1115/1.4007659.

[15] Zhao R, Liu S, Li Z, Liu Y, Li N, Xu P. Exergy, exergoeconomic and carbon emission analysis of a novel biomass pyrolysis system with self-heating and torrefaction. Energy 2024;313. https://doi.org/10.1016/j.energy.2024.133913.

[16] Bilgen S. Correlation for estimation of the chemical availability (exergy) from ultimate analysis of pyrolytic oils obtained from fast pyrolysis of biomass. Energy Sources Part A 2016;38:1286–92. https://doi.org/10.1080/15567036.2014.925990.

[17] Hasan MM, Rasul MG, Jahirul MI, Mofijur M. Fuelling the future: Unleashing energy and exergy efficiency from municipal green waste pyrolysis. Fuel 2024;357. https://doi.org/10.1016/j.fuel.2023.129815.

[18] Tiara ES, Susanto Ginting A, Setiawan RPA, Joelianingsih J, Tambunan AH. Exergy Analysis on Pyrolysis Process of Oil Palm Empty Fruit Bunch. IOP Conf Ser Mater Sci Eng, vol. 557, Institute of Physics Publishing; 2019. https://doi.org/10.1088/1757-899X/557/1/012058.

[19] Li T, Wang J, Chen H, Li W, Pan P, Wu L, et al. Performance analysis of an integrated biomass-to-energy system based on gasification and pyrolysis. Energy Convers Manag 2023;287. https://doi.org/10.1016/j.enconman.2023.117085.

[20] Li R, Song G, Huang D, Hu S, Fantozzi F, Hassan A, et al. Comparative study of process simulation, energy and exergy analyses of solar enhanced char-cycling biomass pyrolysis process. Energy Convers Manag 2024;302. https://doi.org/10.1016/j.enconman.2024.118082.

[21] Elhenawy Y, Fouad K, Bassyouni M, Al-Qabandi OA, Majozi T. Yield and energy outputs analysis of sawdust biomass pyrolysis. Energy Convers Manage: X 2024;22. https://doi.org/10.1016/j.ecmx.2024.100583.

[22] Piazzi S, Patuzzi F, Baratieri M. Energy and exergy analysis of different biomass gasification coupled to Fischer-Tropsch synthesis configurations. Energy 2022;249. https://doi.org/10.1016/j.energy.2022.123642.

[23] Buentello-Montoya D, Zhang X. An energy and exergy analysis of biomass gasification integrated with a char-catalytic tar reforming system. Energy Fuels 2019;33:8746–57. https://doi.org/10.1021/acs.energyfuels.9b01808.

[24] Najar R, Kazemi A, Borji M, Nikian M. Conventional and advanced exergy and exergoeconomic analysis of a biomass gasification based SOFC/GT cogeneration system. J Renewable Sustainable Energy 2023;15:046303. https://doi.org/10.1063/5.0159977.

[25] Saidur R, Boroumandjazi G, Mekhilef S, Mohammed HA. A review on exergy analysis of biomass based fuels. Renew Sustain Energy Rev 2012;16:1217–22. https://doi.org/10.1016/j.rser.2011.07.076.

[26] Cui L, Liu C, Liu H, Zhao W, Zhang Y. Exergy transfer analysis of biomass and microwave based on experimental heating process. Sustainability (Switzerland) 2023;15. https://doi.org/10.3390/su15010388.

[27] Saidur R, Abdelaziz EA, Demirbas A, Hossain MS, Mekhilef S. A review on biomass as a fuel for boilers. Renew Sustain Energy Rev 2011;15:2262–89. https://doi.org/10.1016/j.rser.2011.02.015.

[28] Nhuchhen DR, Abdul SP. Estimation of higher heating value of biomass from proximate analysis: a new approach. Fuel 2012;99:55–63. https://doi.org/10.1016/j.fuel.2012.04.015.

[29] Yu J, Sun L, Berrueco C, Fidalgo B, Paterson N, Millan M. Influence of temperature and particle size on structural characteristics of chars from Beechwood pyrolysis. J Anal Appl Pyrol 2018;130:249–55. https://doi.org/10.1016/j.jaap.2018.01.018.

[30] Dessì F, Mureddu M, Ferrara F, Pettinau A. A comprehensive pathway on the determination of the kinetic triplet and the reaction mechanism of brewer's spent grain and beech wood chips pyrolysis. Renew Energy 2022;190:548–59. https://doi.org/10.1016/j.renene.2022.03.084.

[31] Al-Rumaihi A, Shahbaz M, Mckay G, Mackey H, Al-Ansari T. A review of pyrolysis technologies and feedstock: a blending approach for plastic and biomass towards optimum biochar yield. Renew Sustain Energy Rev 2022;167. https://doi.org/10.1016/j.rser.2022.112715.

[32] Jerzak W, Acha E, Li B. Comprehensive review of biomass pyrolysis: conventional and advanced technologies, reactor designs, product compositions and yields, and techno-economic analysis. Energies (Basel) 2024;17. https://doi.org/10.3390/en17205082.

[33] Jr Harrison JEH. Estimation of liquid and solid heat capacities using a modified Kopp's rule. Chem Eng Commun 1992;112:21–30. https://doi.org/10.1080/00986449208935989.

[34] CRC Handbook of Chemistry and Physics, 2009−2010, 90th ed. J Am Chem Soc 2009;131:12862. https://doi.org/10.1021/ja906434c.

[35] Mcbride BJ, Gordon S, Cleveland A, Reno MA. NASA technical memorandum 4513 coefficients for calculating thermodynamic and transport properties of. Individual Species 1993.

[36] Manganaro J, Chen B, Adeosun J, Lakhapatri S, Favetta D, Lawal A, et al. Conversion of residual biomass into liquid transportation fuel: an energy analysis. Energy Fuels 2011;25:2711–20. https://doi.org/10.1021/ef200327e.

[37] Khan S, Malviya R, Athankar KK. Optimization and simulation of heat loss in pyrolysis reactor. Mater Today Proc Elsevier Ltd 2023;72:2643–59. https://doi.org/10.1016/j.matpr.2022.08.285.

[38] Dincer I, Rosen MA. Exergy: Energy. Environment and Sustainable Development: Elsevier Science; 2012.

[39] Szargut J. Exergy method: technical and ecological applications. vol. 18. WIT press; 2005.

[40] Hepbasli A. A key review on exergetic analysis and assessment of renewable energy resources for a sustainable future. Renew Sustain Energy Rev 2008;12:593–661. https://doi.org/10.1016/j.rser.2006.10.001.

[41] Shieh JH, Fan LT. Estimation of energy (enthalpy) and exergy (availability) contents in structurally complicated materials. Energy Source 1982;6:1–46. https://doi.org/10.1080/00908318208946020.

[42] Rao MS, Singh SP, Sodha MS, Dubey AK, Shyam M. Stoichiometric, mass, energy and exergy balance analysis of countercurrent fixed-bed gasification of post-consumer residues. Biomass Bioenergy 2004;27:155–71. https://doi.org/10.1016/j.biombioe.2003.11.003.

[43] Kaushik SC, Singh OK. Estimation of chemical exergy of solid, liquid and gaseous fuels used in thermal power plants. J Therm Anal Calorim 2014;115:903–8. https://doi.org/10.1007/s10973-013-3323-9.
[44] Di Blasi C. Modeling chemical and physical processes of wood and biomass pyrolysis. Prog Energy Combust Sci 2008;34:47–90. https://doi.org/10.1016/j.pecs.2006.12.001.
[45] Aysu T, Küçük MM. Biomass pyrolysis in a fixed-bed reactor: effects of pyrolysis parameters on product yields and characterization of products. Energy 2014;64:1002–25. https://doi.org/10.1016/j.energy.2013.11.053.
[46] Tabal A, Belyazid O, Dahman H, Berrich E, Jeguirim M, El Achaby M, et al. Intermediate pyrolysis of Ficus nitida wood in a fixed-bed reactor: effect of pyrolysis parameters on bio-oil and bio-char yields and properties. C R Chim 2023;26. https://doi.org/10.5802/crchim.253.
[47] Vieira FR, Romero Luna CM, Arce GLAF, Ávila I. Optimization of slow pyrolysis process parameters using a fixed bed reactor for biochar yield from rice husk. Biomass Bioenergy 2020;132. https://doi.org/10.1016/j.biombioe.2019.105412.
[48] Cong H, Meng H, Mašek O, Yao Z, Li L, Yu B, et al. Comprehensive analysis of industrial-scale heating plants based on different biomass slow pyrolysis technologies: product property, energy balance, and ecological impact. Clean Eng Technol 2022;6. https://doi.org/10.1016/j.clet.2021.100391.
[49] Indrawan N, Kumar A, Moliere M, Sallam KA, Huhnke RL. Distributed power generation via gasification of biomass and municipal solid waste: a review. J Energy Inst 2020;93:2293–313. https://doi.org/10.1016/j.joei.2020.07.001.
[50] Bridgwater T. Challenges and opportunities in fast pyrolysis of biomass: part I. Johnson Matthey Technol Rev 2018;62:118–30. https://doi.org/10.1595/205651318X696693.
[51] Sahoo SS, Vijay VK, Chandra R, Kumar H. Production and characterization of biochar produced from slow pyrolysis of pigeon pea stalk and bamboo. Clean Eng Technol 2021;3. https://doi.org/10.1016/j.clet.2021.100101.
[52] Kambo HS, Dutta A. A comparative review of biochar and hydrochar in terms of production, physico-chemical properties and applications. Renew Sustain Energy Rev 2015;45:359–78. https://doi.org/10.1016/j.rser.2015.01.050.
[53] Atienza-Martínez M, Ábrego J, Mastral JF, Ceamanos J, Gea G. Energy and exergy analyses of sewage sludge thermochemical treatment. Energy 2018;144:723–35. https://doi.org/10.1016/j.energy.2017.12.007.
[54] Peters JF, Petrakopoulou F, Dufour J. Exergetic analysis of a fast pyrolysis process for bio-oil production. Fuel Process Technol 2014;119:245–55. https://doi.org/10.1016/j.fuproc.2013.11.007.
[55] Ding HS, Jiang H. Self-heating co-pyrolysis of excessive activated sludge with waste biomass: energy balance and sludge reduction. Bioresour Technol 2013;133:16–22. https://doi.org/10.1016/j.biortech.2013.01.090.
[56] Bacovsky D, Dißauer C, Drosg B, Kuba M, Matschegg D, Schmidl C. IEA Bioenergy. 2022.
[57] Polin JP, Peterson CA, Whitmer LE, Smith RG, Brown RC. Process intensification of biomass fast pyrolysis through autothermal operation of a fluidized bed reactor. Appl Energy 2019;249:276–85. https://doi.org/10.1016/j.apenergy.2019.04.154.
[58] Chavando A, Silva VB, Tarelho LAC, Cardoso JS, Eusebio D. Simulation of a continuous pyrolysis reactor for a heat self-sufficient process and liquid fuel production. Energies (Basel) 2024;17. https://doi.org/10.3390/en17143526.
[59] Cavalloni FC, Strassburg J, Lustenberger D, Griffin T. Oxidative pyrolysis for variable heating output with wood pellets. Energies (Basel) 2025;18. https://doi.org/10.3390/en18071702.
[60] Amari T, Tanaka M, Koga Y, Okuno S, Tajima A. 204 biomass solid fuel from sewage sludge with pyrolysis and co-firing in coal power plant. Proc Symp Environ Eng 2006;2006(16):151–3. https://doi.org/10.1299/jsmeenv.2006.16.151.
[61] Milhé M, Van De Steene L, Haube M, Commandré JM, Fassinou WF, Flamant G. Autothermal and allothermal pyrolysis in a continuous fixed bed reactor. J Anal Appl Pyrolysis, vol. 103, Elsevier B.V.; 2013, p. 102–11. https://doi.org/10.1016/j.jaap.2013.03.011.
[62] Han K-H, Yun S-I, Kwak J-H, Lee S-I. A review on international carbon credit certification methodologies for biochar as a soil amendment. Korean J Soil Sci Fert 2023;56:572–94. https://doi.org/10.7745/kjssf.2023.56.4.572.
[63] Chiaramonti D, Lehmann J, Berruti F, Giudicianni P, Sanei H, Masek O. Biochar is a long-lived form of carbon removal, making evidence-based CDR projects possible. Biochar 2024;6. https://doi.org/10.1007/s42773-024-00366-7.
[64] Islam S, Dincer I. A comparative study of syngas production from two types of biomass feedstocks with waste heat recovery. J Energy Resour Technol Trans ASME 2018;140. https://doi.org/10.1115/1.4039873.
[65] Brown RC. Process intensification through directly coupled autothermal operation of chemical reactors. Joule 2020;4:2268–89. https://doi.org/10.1016/j.joule.2020.09.006.
[66] Huang Y, Li B, Liu D, Xie X, Zhang H, Sun H, et al. Fundamental advances in biomass autothermal/oxidative pyrolysis: a review. ACS Sustain Chem Eng 2020;8:11888–905. https://doi.org/10.1021/acssuschemeng.0c04196.
[67] Greco G, Di Stasi C, Rego F, González B, Manyà JJ. Effects of slow-pyrolysis conditions on the products yields and properties and on exergy efficiency: a comprehensive assessment for wheat straw. Appl Energy 2020;279. https://doi.org/10.1016/j.apenergy.2020.115842.
[68] Wang X, Lv W, Guo L, Zhai M, Dong P, Qi G. Energy and exergy analysis of rice husk high-temperature pyrolysis. Int J Hydrogen Energy 2016;41:21121–30. https://doi.org/10.1016/j.ijhydene.2016.09.155.